Tectonophysics, 78 (1981) 527—543.
Elsevier Scientific Publishing Company, Amsterdam — Printed in The Netherlands

DEFORMATION EXPERIMENTS ON ANHYDRITE ROCKS OF DIFFERENT GRAIN SIZES: RHEOLOGY AND MICROFABRIC

W.H. MÜLLER, S.M. SCHMID and U. BRIEGEL
Geological Institute, Swiss Federal Institute of Technology, ETH, Zürich (Switzerland)
(Received January 26, 1981)

ABSTRACT

Müller, W.H., Schmid, S.M. and Briegel, U., 1981. Deformation experiments on anhydrite rocks of different grain sizes: Rheology and microfabric. In: G.S. Lister, H.-J. Behr, K. Weber and H. Zwart (Editors), The Effect of Deformation on Rocks. Tectonophysics, 78: 527—543.

Three anhydrite rocks of different grain size were experimentally deformed in the 20° to 450°C temperature range. The strength of the fine-grained varieties becomes strongly temperature and strain-rate dependent above 300°C and a flow law of the form $\dot{\epsilon} = A \cdot \exp(-H/RT) \cdot [\sinh(\sigma/\sigma_0)]^n$ with an activation energy H, of 27—36 kcal · mole^{-1} and a very low value for the exponent n of 1.5—2 was found. The course-grained rock remains relatively insensitive to strain rate and temperature even at 450°C. Microstructural and X-ray texture analyses suggest that intracrystalline glide and twinning are the major deformation mechanisms. The transition from strong work hardening, observed at high stresses, into steady-state flow at low stresses was found to correlate with the onset of dynamic recrystallization by grain boundary migration.

INTRODUCTION

In geological environments anhydrite rocks are known to deform in a rather ductile manner even at relatively low temperatures. Together with other evaporites, notably halite and gypsum, they often form detachment horizons. A well-documented case is the décollement of the Jura folds from the underlying basement commonly thought to be virtually undeformed (Buxtorf, 1907; Laubscher, 1961) along the evaporite formations of middle and upper Triassic age. Because halite occurs in isolated lenses only and becuase gypsum is not stable at greater depth (Berner, 1971) anhydrite rocks together with intercalated shaly horizons must be the major mechanically effective constituent of this décollement horizon. Ductile folding in this anhydrite formation has been recorded by Laubscher (1975).

This field evidence apparently conflicts with earlier experimental work on anhydrite at room temperature by Handin and Hager (1957) and at temperatures up to 300°C by Müller and Siemes (1974) indicating that anhydrite is

0040-1951/81/0000—0000/$02.50

about as strong as calcite rocks under laboratory strain rates. New work on different anhydrite rocks revealed a strong influence of grain size on the strength at room temperature; fine-grained aggregates were found to be significantly stronger (Müller and Briegel, 1977). Later the investigations were extended to higher temperatures (up to 450° C) on a finer-grained variety (the Riburg variety). It was found that flow of fine-grained anhydrite above 300° C became strongly temperature and strain-rate dependent (Müller and Briegel, 1978, 1980).

This study extends the existing experimental work in two directions: (1) new rheological results on a coarse-grained variety will be presented and discussed in relation to already published data with emphasis on the role of grain size on the strength; and (2) microfabric investigations on the experimentally deformed material are presented as a basis for comparison with naturally deformed anhydrite.

STARTING MATERIAL AND TECHNIQUES

The deformation experiments were performed in an externally heated pressure vessel described in Müller and Briegel (1977). Oven-dried cores of 24 mm length and 12 mm diameter were sealed in a copper jacket and deformed under 1.5 kbar confining pressure unless stated otherwise. The following blocks of material were used:

AWP: This fine-grained variety was taken from a drillhole in the Table Jura of Switzerland (Wandflue). The rock exhibits a strong planar anisotropy containing a weakly developed lineation. The cores were compressed parallel to the lineation. The average grain size in this very pure anhydrite rock was determined by counting the number of grain boundary intersections along traverses parallel and perpendicular to the foliation to be around 20 μm. Individual grains commonly vary between 20 and 100 μm in length and between 5 and 25 μm in width.

AR: This variety with a medium grain size was obtained from another drillhole in the Table Jura (Riburg). It contains tabular grains with no preferred shape orientation. Apart from anhydrite (91%) minor amounts of dolomite and gypsum occur. The average grain size is around 100 μm and the grains vary between 160 and 600 μm in length and between 30 and 300 μm in width.

AVC: This coarse-grained rock crops out in the Piora synform south of the Gotthard massif. Very impure specimens were used in the room temperature experiments reported by Müller and Briegel (1977). The material used for the high-temperature tests presented here consists of about 90% anhydrite and minor amounts of gypsum, dolomite, magnesite, phlogopite and talc. The average grain size is around 600 μm. The deformation experiments were

carried out at constant strain rate. At the end of some of the tests the stress was allowed to relax and the stress vs. time curve was used to obtain further information on the strain rate vs. stress relationship (more details are given in Müller and Briegel, 1978).

For microstructural studies polished thin sections of 5—15 μm thickness were prepared by using alcohol as a grinding liquid and diamond paste for polishing.

The texture was determined on a Scintag-Seiffert texture goniometer operating in transmission mode using Co-radiation. Pole profiles (pole density of the diffracting plane as a function of the angle between shortening direction and the direction of the normal to the diffracting plane) were recorded on the following 13 reflections of anhydrite: 111, 002/020, 200, 210, 022, 202/220, 212, 113, 301, 230, 232, 133 and 024/042. For indexing we chose the setting with $a < b < c$. The intensity contributions from each component in the case of the three combined peaks were calculated from the structure factors determined by Höhne (1963). The inverse pole figures for the shortening direction were calculated, using a 12th order expansion with a FORTRAN program described by Casey (1981, this volume).

RHEOLOGY

Some representative stress-strain curves for all the three anhydrite rocks investigated are summarized in Fig. 1. All samples at 300°C exhibit work hardening (Fig. 1a). Only the fine-grained AR and AWP samples deform in steady state at the higher temperatures (Fig. 1b). This transition into steady state is also indicated in Fig. 3 and occurs below flow stresses (at 10% strain) of between 1500 and 2000 bars.

Figure 2 illustrates the influence of initial grain size on the strength at 10% strain. Note that both increasing temperature and decreasing strain rate bring about a change in the influence of a smaller grain size from a hardening effect at high stresses into a softening effect at low stresses. This indicates a change in the deformation mechanism which will be discussed in a later section. Similar observations on opposite effects of grain size on the strength were made on limestones (Schmid, 1976; Schmid et al. 1981).

Figure 3 illustrates the strength at 10% strain as a function of strain rate at 300°C. The curves in this figure concerning the AWP and AR specimens represent a best fit for the results from constant strain rate and stress relaxation tests. The list of experiments and data points are published elsewhere (Müller and Briegel, 1978, for the AR specimens; Müller and Briegel, 1980, for the AWP specimens). The flow law giving a best fit was found to be of the form:

$$\dot{\epsilon} = A \cdot \exp\left[\frac{-H}{RT}\right] \cdot \left[\sinh \frac{\sigma}{\sigma_o}\right]^n \qquad (1)$$

where A, H, σ_o, and n are parameters listed in Table I. Such an empirical hy-

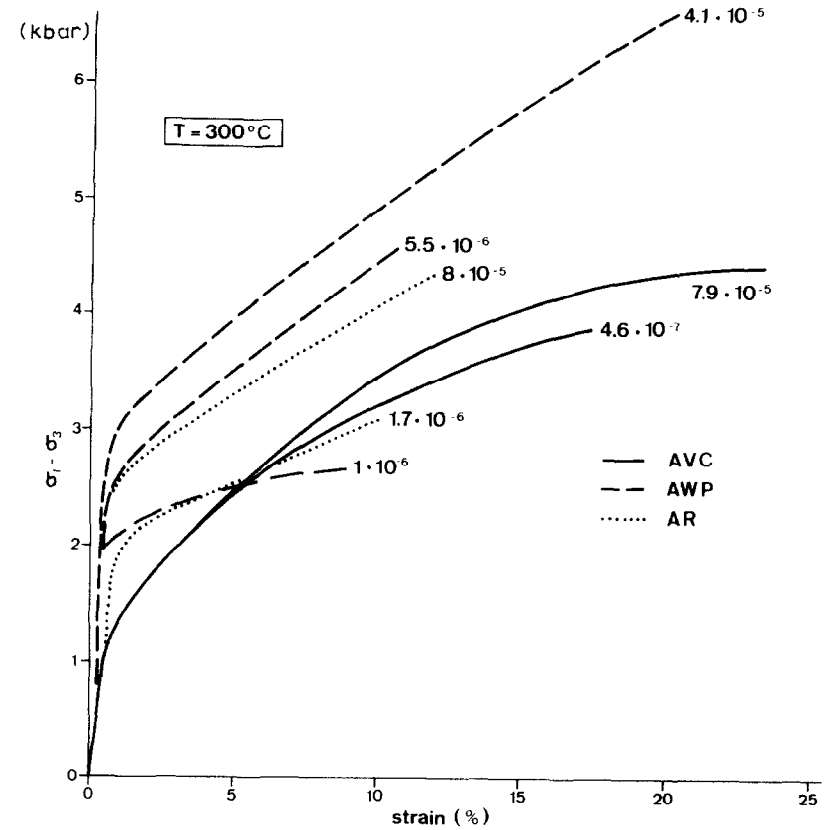

Fig. 1. Stress-strain curves of anhydrite specimens deformed at 300°C (a) and 450°C (b), all at 1.5 kbar confining pressure.

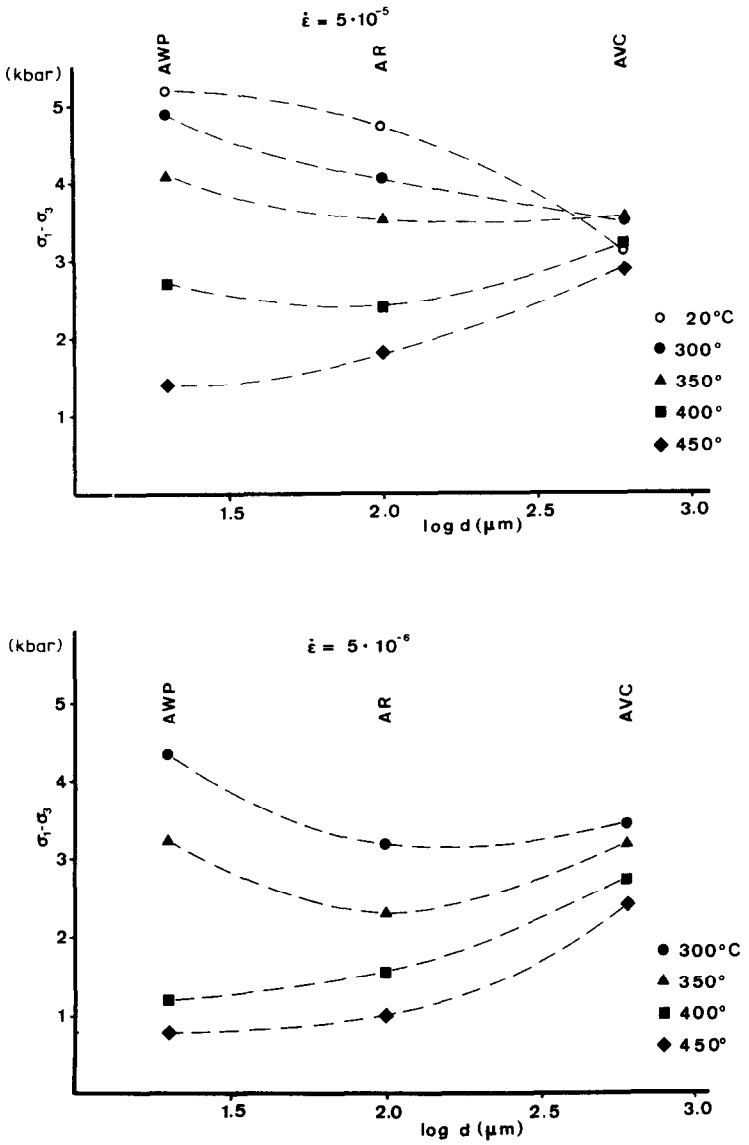

Fig. 2. The strength at 10% strain as a function of grain size at strain rates of 5×10^{-5} sec^{-1} (a) and 5×10^{-6} sec^{-1} (b).

perbolic sine law (Garofalo, 1965) corresponds to a power law ($\dot{\varepsilon}\alpha = \sigma^n$) with a continuously changing value of n above stresses greater than the value of σ_o. No flow law was fitted to the rather scattered data values from the AVC specimens listed in Table II. In order to represent these new data in the synoptic diagram of Fig. 3, an activation energy of 36.4 kcal $mole^{-1}$ (the value for the AR specimens) was used in calculating the strain rates at 300°C (data

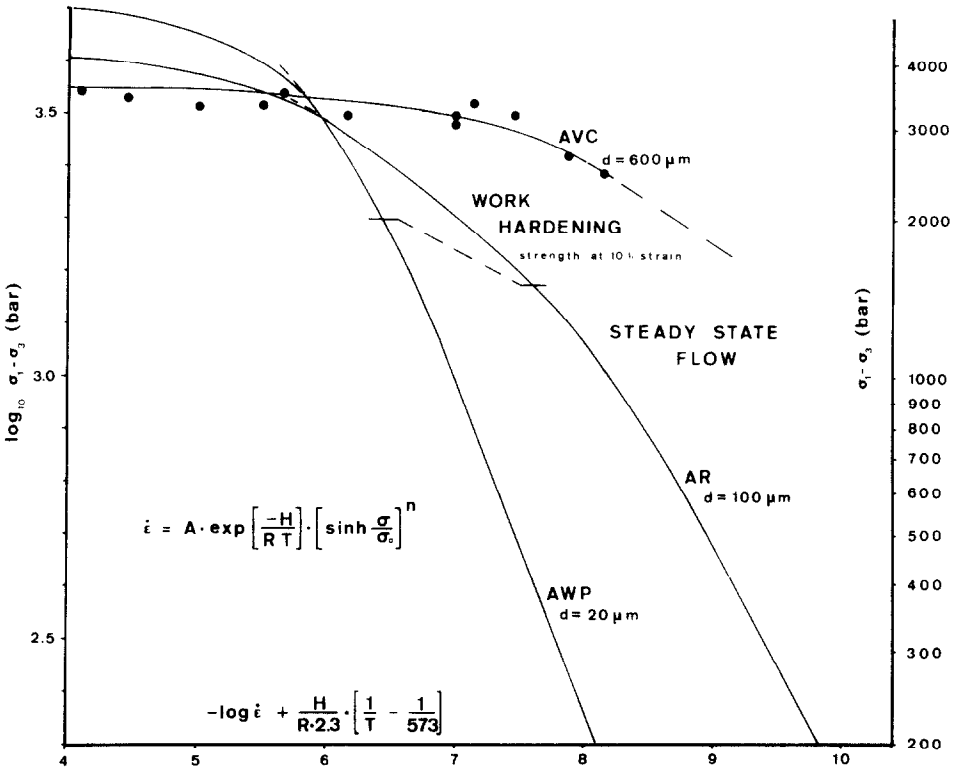

Fig. 3. Synoptic diagram in the form of a log-log plot of the strength at 10% strain vs. the strain rate at about 300°C. The best fit curves for the AWP and AR specimens correspond to the values for the various constants in the hyperbolic sine law listed in Table I, the data points for the AVC specimens are listed in Table II.

points in Fig. 3). The best fit curve shown for the AVC specimens is a visual best fit and does not represent a specific form of the flow law.

The hyperbolic sine flow law chosen closely corresponds to a power law at stresses below a value of σ_0 in eq. 1. Thus, a power law with the very low exponent of 1.5 and 2 could be fitted equally well for a region below differential stresses of 1700 and 800 bar for the AWP and AR specimens, respec-

TABLE I

Best fit values of the parameters in eq. 1

	A (sec^{-1})	H (kcal $mole^{-1}$)	σ_0 (bar)	n
AWP	6.03×10^3	27.3	1700	1.5
AR	2.07×10^5	36.4	800	2

TABLE II

List of experiments on the coarse grained anhydrite AVC

Experiment Nr.	Temperature °C	Differential stress at 10% strain (bar)	Strain rate (sec^{-1})
AVC 58	300	3480	7.9×10^{-5}
AVC 59	300	3390	3.5×10^{-5}
AVC 60	300	3380	8.8×10^{-6}
AVC 61	300	3370	3.1×10^{-6}
AVC 52	350	3220	4.6×10^{-7}
AVC 65	350	3480	3.1×10^{-5}
AVC 66	350	3340	9.7×10^{-7}
AVC 62	400	3230	8.2×10^{-5}
AVC 64	400	3180	1.2×10^{-5}
AVC 51	450	3040	8.0×10^{-5}
AVC 54	450	2660	1.1×10^{-5}
AVC 56	450	2450	5.5×10^{-6}

tively. This very low value for n is unusual for rocks and similarly low values of n were only found in fine-grained Solnhofen limestone deforming by a mechanism of grain boundary sliding (Schmid et al., 1977) at substantially higher temperatures. Calcite and anhydrite have a similar melting point (1430°C for anhydrite) and the observation of such a low value of n at a homologuous temperature (T/T_m) of only 0.42 in the case of anhydrite is highly unusual.

The fine-grained variety AWP exhibits a lower value for both the activation energy and the exponent n compared to the coarser-grained variety AR (Table I). The question of how much factors other than just grain size determine the flow behavior of a polycrystalline aggregate remains open in the case of both calcite and anhydrite.

All the data reported so far were obtained at 1.5 kbar confining pressure. Müller and Briegel (1977) have shown that the strength of all the three rocks is strongly dependent on confining pressure at room temperature. At 400°C the strength of both AWP and AR specimens is insensitive to confining pressure whereas the AVC specimens are still pressure sensitive over the entire range of confining pressures up to 3 kbar. This is noteworthy here because it shows that a component of cataclastic flow can be ruled out for the AR and AWP specimens at the higher temperatures; the dependence of flow stress on confining pressure is a useful diagnostic feature for cataclastic flow (Paterson, 1978). It also indicates that the transition into fully crystal plastic flow is favoured by a small grain size.

MICROFABRIC

Optical microstructure

Anhydrite grains of specimens deformed at room temperature exhibit undulatory extinction. This indicates that the deformation mechanism is not only exclusively of a cataclastic nature, although a component of cataclastic flow is indicated by the strong influence of confining pressure on the strength reported in the previous section. Direct evidence for cataclasis cannot be seen in the microstructures except in the region of the brittle-ductile transition where distinct shear planes develop. These shear planes are accompanied by an aggregate of microcrystalline anhydrite which appears to be the product of cataclastic grain fragmentation. In contrast to the high-temperature experiments twinning is extremely scarce or absent, indicating that translation gliding alone is responsible for the crystal plastic fraction of total strain. The latter observation agrees with the findings of Ramez (1976a, b) and suggests that the critical resolved shear stress for twinning is higher than that for translation gliding at room temperature.

At the higher temperatures twinning is the dominant microstructural feature in weakly deformed specimens or in a wedge-shaped region of low strain near the pistons in specimens deformed to more than 20% strain (Figs. 4, 5, 8, 9, 10). At large strains twinning goes to completion and such a sequence from low to high strains is illustrated by Figs. 4—6. The micrograph of Fig. 4 was taken in the immediate vicinity of the piston and it shows that less than 50% of the volume of grains suitable oriented for twinning is in the twinned orientation [1]. Further away from the piston (Fig. 5) lamellae or insular domains are in a still untwinned orientation and make up a small volume fraction of a grain. Figure 5 exhibits signs of twin boundary migration (bulging of twin boundaries) suggesting that twinning goes near completion by a combined process of lattice reorientation by shear twinning and twin boundary migration. The micrograph of Fig. 6, taken from the central portion of the same specimen, finally shows a completely changed microstructure and no twins are visible anymore.

Figure 6 also shows that the average grain size is drastically reduced by dynamic recrystallization and this feature is restricted to specimens deformed at higher temperatures in a region of steady-state flow. The sutured nature of the grain boundaries strongly suggests a mechanism of recrystallization by grain boundary migration (Guillope and Poirier, 1979) rather than a mechanism of nucleation and growth of new grains or of subgrain rotation. Fig-

[1] If the direction of shortening is known it is easy to decide on twinned and untwinned portions of a grain by inserting a gypsum plate. As shown in the inverse pole figure of Fig. 12f the direction of the *c*-axis (parallel to the *X* optical direction) is near to the shortening direction before twinning and swings around by nearly 90° such that the *a*-axis (parallel to the *Z* optical direction) now becomes aligned with the shortening direction.

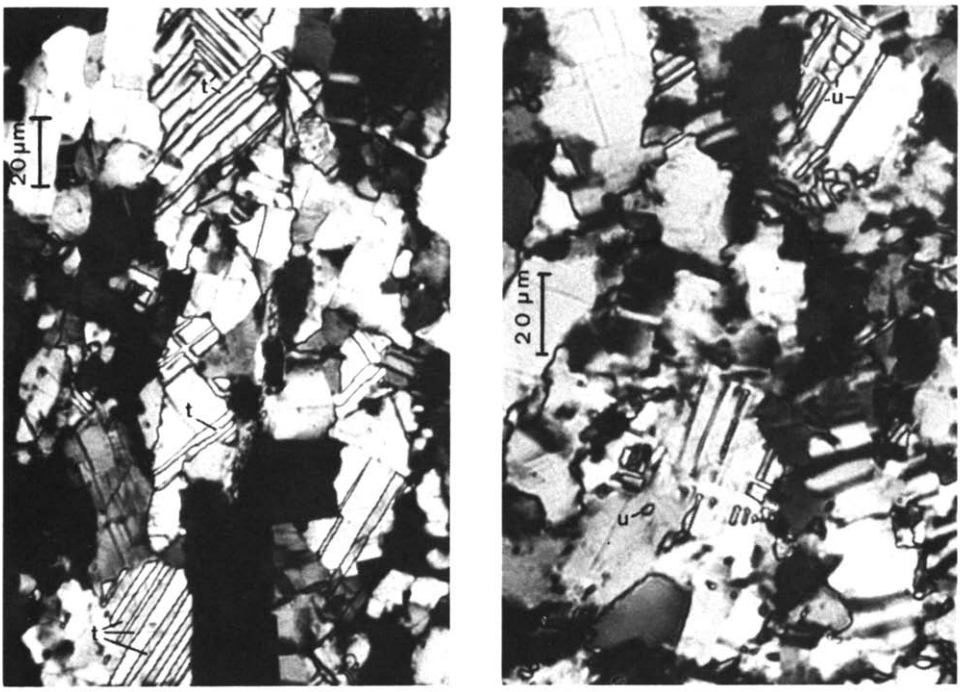

Fig. 4. Optical micrograph of specimen AWP 98 deformed at 450°C, 4.5×10^{-5} sec^{-1}, 50% shortening. The micrograph is taken in the vicinity of the piston, where the strain is locally very small. Note that only small portions of a grain are in a twinned orientation (marked *t*). The compression axis is N—S in this and all the following micrographs.

Fig. 5. Specimen AWP 98, further away from the piston in a region of higher strain as compared to Fig. 4. Note that the thin lamellae and insular domains (marked *u*) are in a still untwinned orientation.

ure 9 illustrates the consumption of old twinned grains by this process of recrystallization in a specimen of the AR variety.

Figure 7 is representative for the microstructure at high strains for AWP and AR specimens at lower temperatures where work hardening continues up to high strains. The high degree of undulous extinction and the absence of a pervasive dynamic recrystallization are obvious. In both this high-stress region and at low stresses, where steady-state is observed, no subgrain formation could be observed, possibly because the subgrains are too small to be optically detectable. In view of what can be seen optically it is tempting to associate the steady-state behaviour observed at the low stresses with the ability of the aggregate to recrystallize by a grain boundary migration mechanism opposing work hardening by eliminating grains of high stored strain energy.

The microstructural features of the AR and AWP specimens are very similar. The coarse-grained AVC specimens, however, do not show much evi-

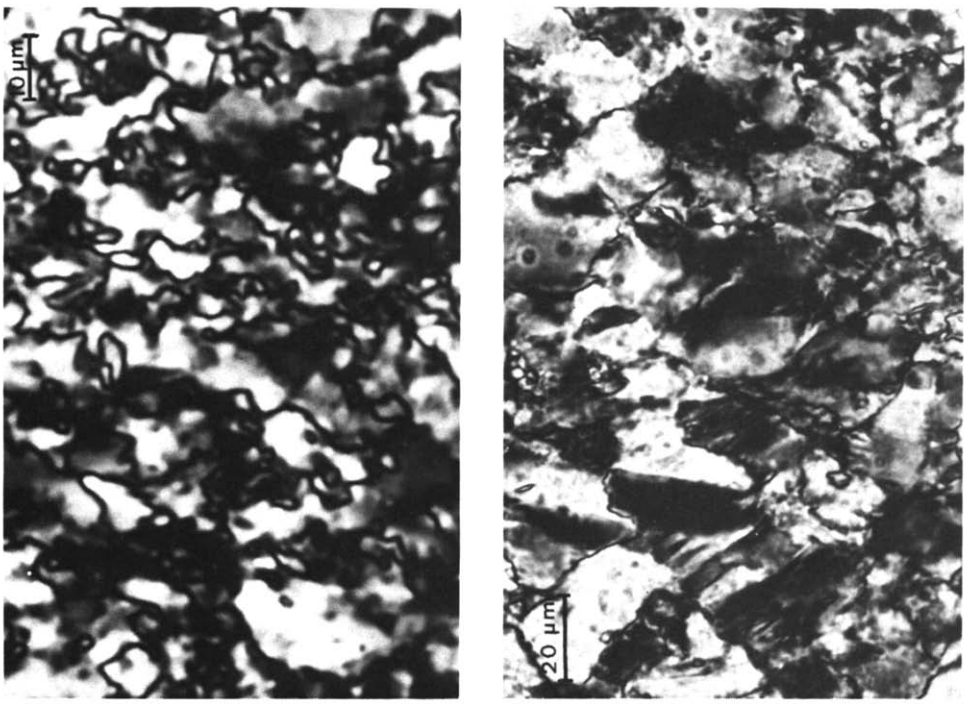

Fig. 6. The same specimen AWP 98 in the central portion of the cylinder where shortening is in excess of 50%. Note the highly serrated grain boundaries indicative for grain boundary migration completely transforming the old microstructure.

Fig. 7. Specimen AWP 97 deformed at 300°C, 1×10^{-5} sec^{-1}, 34% shortening. This central part of the cylinder shows strong undulouse extinction and no significant amounts of recrystallization by grain boundary migration in comparison with Fig. 6.

dence for grain boundary migration even at 450°C (Fig. 10). Twins and deformation bands are the obvious deformation traces (Fig. 11). The fact that no steady-state flow was observed in this coarse-grained variety again supports the idea that steady-state flow is associated with the ability of the aggregate to undergo dynamic recrystallization.

The profound effect of annealing on the microstructure is illustrated by Fig. 5. Grain boundaries rearrange into low-energy configurations with straight grain boundaries. Many of the grains appear twinned along a single straight twin boundary. This suggests that any study on the microstructure of naturally deformed anhydrite should consider the possibility of such annealing effects.

X-RAY TEXTURE ANALYSIS

Eleven specimens of the finest-grained variety AWP and one specimen of the AR variety were analyzed. Two specimens deformed at room tempera-

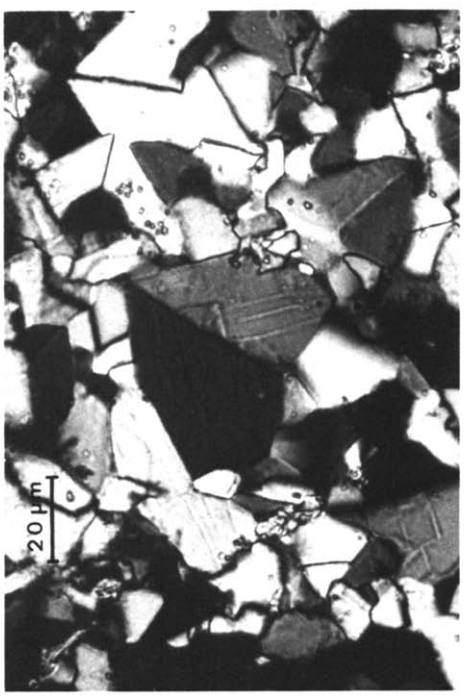

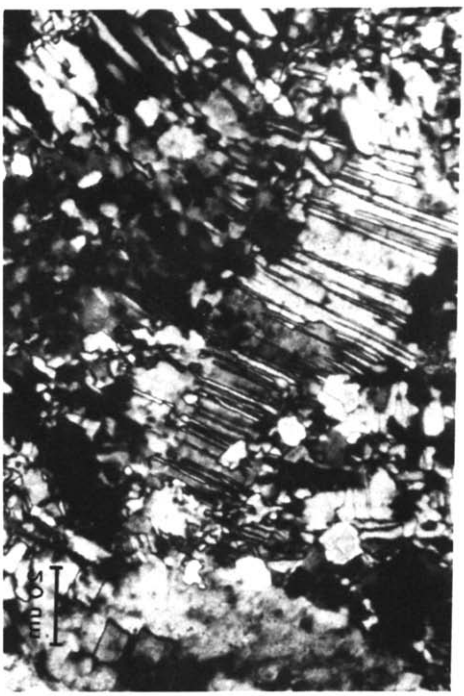

Fig. 8. Specimen AWP 99 deformed at 350°C, 5×10^{-6} sec^{-1}, 25% shortening. This specimen was subsequently annealed for 7 hours at 450°C. Note the straight grain and twin boundaries in many of the grains.

Fig. 9. Specimen AR 43 deformed at 400°C, 8×10^{-6} sec^{-1}, 15% shortening. Old twinned grains are being consumed by a recrystallized matrix.

ture gave weak non-reproducable textures probably reflecting an initial texture. All specimens between 300°C and 450°C exhibit the same type of texture regardless of the presence or absence of dynamic recrystallization. This texture is characterized by a high concentration of compression axes parallel to the poles to (100) and a strong depletion in all regions at a high angle to the (100) pole. The two inverse pole figures of Fig. 12a, b, are representative for all the other measured specimens as well and illustrate the development from medium (Fig. 12a) to high strains (Fig. 12b). The intensity of the texture remains nearly unchanged but the high-concentration area broadens towards (210) at the expense of an area between (101) and (001). The annealed specimen described in the earlier section (compare Fig. 8) exhibits a weaker texture which is qualitatively of the same type (Fig. 12c). Thus, although the microstructure changed as a consequence of annealing, the characteristic texture is retained, although weakened.

Our findings are in agreement with the pole profiles for the (210) and (002/020) reflections analyzed by Müller and Siemens (1974) in anhydrite

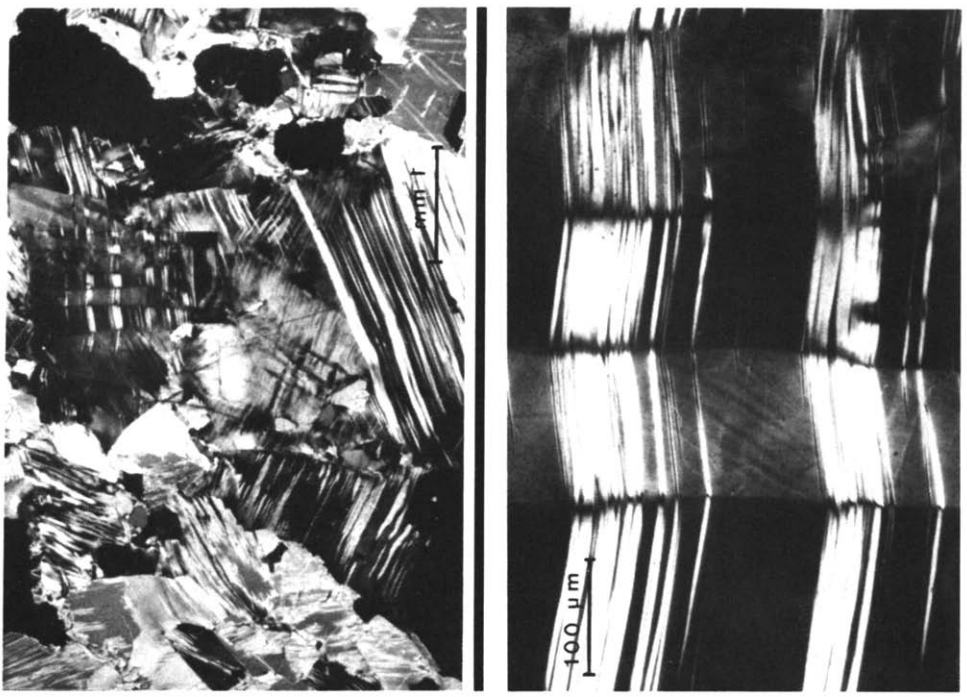

Fig. 10. Specimen AVC 56 deformed at 450°C, 5×10^{-6} sec^{-1}, 15% shortening.

Fig. 11. Detail from Fig. 10. The EW trending deformation bands are interpreted to have formed after twinning on (101) (N—S direction) and as a consequence of translation glide on (012). The diagonally oriented deformation lamellae visible near the center of the micrograph have been found to be oriented parallel to (012).

experimentally deformed at 300°C. Ramez (1976b) determined the following slip systems to be active in experimentally deformed anhydrite:

(1) Translation glide on (001) [010].

(2) Translation glide on (012) with two possible glide directions $[\bar{1}\bar{2}1]$ and $[1\bar{2}1]$ and with a positive sense of gliding only.

(3) Twinning on (101) parallel to the edge of (101) : (010) and a negative sense of shear.

The coefficients of resolved shear stresses for these slip systems have been contoured in Fig. 12d, e, f and allow an empirical interpretation of our texture:

Both glide systems are practically inoperative for compression directions between (001) and (100). Therefore, grains with their compression axis between (001) and (100) are stable orientations in respect to glide. This fact, together with an expected tendency for the grains deforming by the (001) and (012) glide systems to rotate such that the coefficients of resolved shear stress become reduced, will cause a high concentration of compression axes

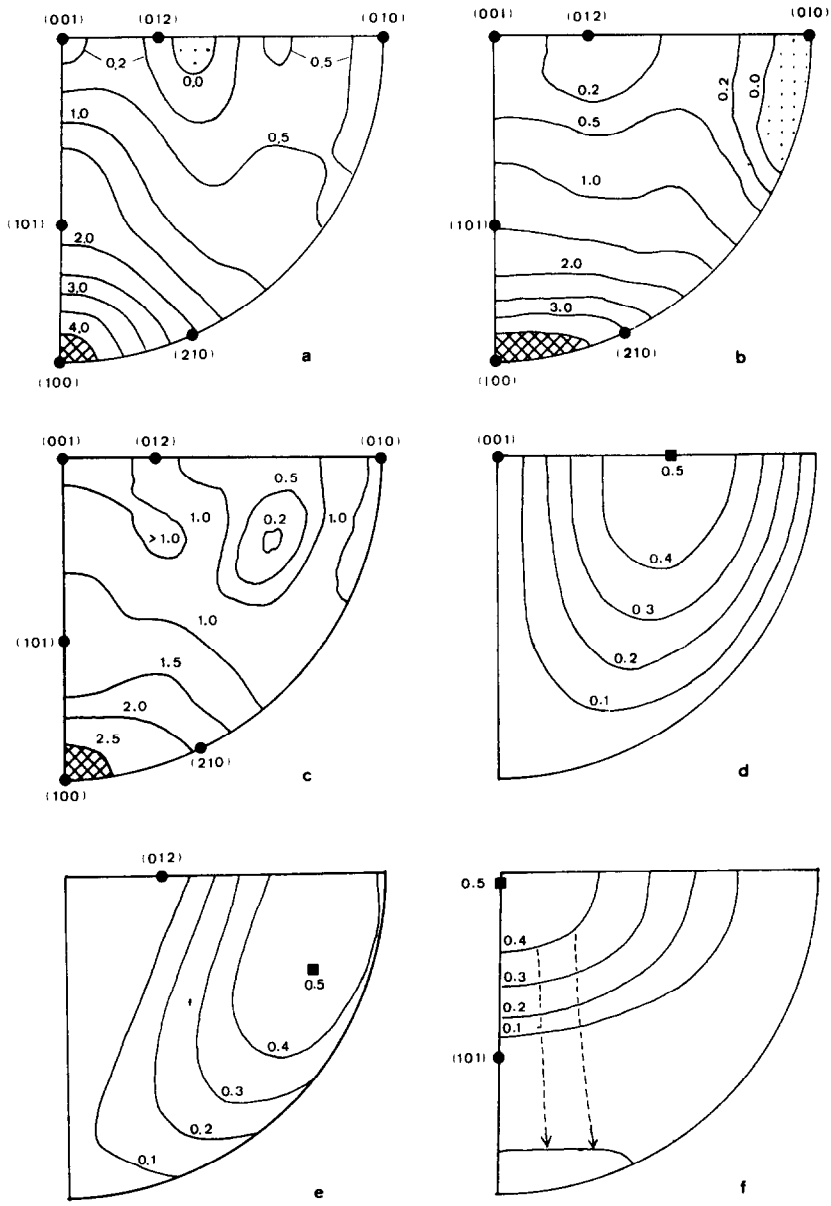

Fig. 12. a. Inverse pole figure (IPF) of the shortening direction for AWP 52 deformed at 450°C, 5×10^{-5} sec^{-1}, 15% shortening.
b. IPF for specimen AWP 98 (compare figs. 4—6) deformed under the same conditions to 50% shortening.
c. IPF for the annealed specimen AWP 99 (for details see fig. 8 and text).
d, e and f. Inverse pole figures of anhydrite contoured for the coefficients of resolved shear stress of the following glide systems: translation glide on (001) in (d), translation glide on (012) in (e) and finally twinning on (101) in (f). In Fig. 12f, the path of points along the 0.4 contour from an untwinned into a twinned position is illustrated by the broken arrows.

in an elongate area between (001) and (100) at the expense of orientation near (010).

Only twinning, however, can bring about the depletion of compression axes near (001). Twinning on (101) rotates the orientation of (001) in the twinned domain through 83.5° around an axis parallel to the (010) pole while the angle of shear amounts to a mere 12.5° (Klassen-Neklyudova, 1964). This twinning is relatively inefficient in accommodating large strains and causing external rotation but it is an extremely powerful reorienting mechanism in terms of creating volume in a twinned orientation. Grains with the compression axis near (001) become twinned (Fig. 12f) and the twinned areas now have their compression axes near (100). It is known for calcite as well that the creation of twinned areas leads to a rapid development of the texture (Casey et al., 1978; Spiers, 1979). The microstructural evidence showed that twinning in anhydrite goes almost to completion in many of the grains after only 20% shortening, in contrast to calcite where most grains are less than 50% twinned (Spiers, 1979; Schmid et al. 1980). This explains the even more rapid development of a strong texture in anhydrite. Since after about 20% strain the favourably oriented grains are twinned, further strain has little effect on strengthening the already formed texture.

It can thus be concluded that twinning is the major mechanism responsible for the strong maximum near (100) and that external rotation as a consequence of glide on (001) and (012) is responsible for the depletion of compression axes near (010).

CONCLUSIONS ON THE DEFORMATION MECHANISMS AND GEOLOGICAL APPLICATIONS

Apart from the room temperature experiments, where a component of cataclasis contributes to total strain and where twinning is absent, the entire range of stresses covered in the 300° to 450°C experiments is characterized by intragranular deformation by twinning and glide. The transition from the work-hardening region at high stresses into the steady state region at low stresses is associated with the appearance of dynamic recrystallization by a grain boundary migration mechanism. The texture indicates that no change in the relative activity of the glide systems occurs. Thus, we propose that the continuously increased importance of dynamic recrystallization causes the gradual reduction in the slope $n = \delta \log \dot{\varepsilon}/\delta \log \sigma$ in Fig. 3.

The grain size dependence of strength at low temperatures in the sense of a hardening effect of a smaller grain size follows the trend observed in other materials and is sometimes referred to as the Hall Petch relationship in metallurgy (Nicolas and Poirier, 1976). It can be related to the hardening effect of grain boundaries which act as obstacles to the free propagation of dislocations.

The opposite (weakening) effect of a small grain size at the higher temperatures is usually explained by the enhanced diffusivity and the shorter dif-

fusion distances in a fine-grained aggregate deforming by diffusion creep (Coble creep) or by diffusion accommodated grain boundary sliding (here a small grain size additionally favours low stresses because grain boundary sliding is more efficient in smaller-grained aggregates). In our case we propose that the weakening effect is generated by the enhanced ability of a fine-grained aggregate to oppose work hardening through a process of grain boundary migration. No evidence for diffusional creep or grain boundary sliding was found. Whether creep of anhydrite in the low stress area, characterized by a low value for the exponent n and a strong grain size sensitivity of flow stress should be referred to as superplastic flow is a semantic problem. It is important to note, however, that no evidence for grain boundary sliding was found in contrast to the behaviour referred to as superplastic flow in limestones (Schmid et al., 1977).

Figure 13 shows the expected strength of anhydrite at geological strain rates based on the assumption that the same deformation mechanism is active in a geological environment. It indicates that although anhydrite has a high strength at room temperature, fine-grained aggregates weaken rapidly above temperatures of 100° to 200°C depending on grain size and strain rate. Mechanical implications for the décollement of the Jura folds based on this extrapolation are discussed elsewhere (Müller and Briegel, 1980; Müller and Hsü, 1980).

The question as to whether the extrapolation based on the experimental results is justified or not remains to be answered by the study of micro-

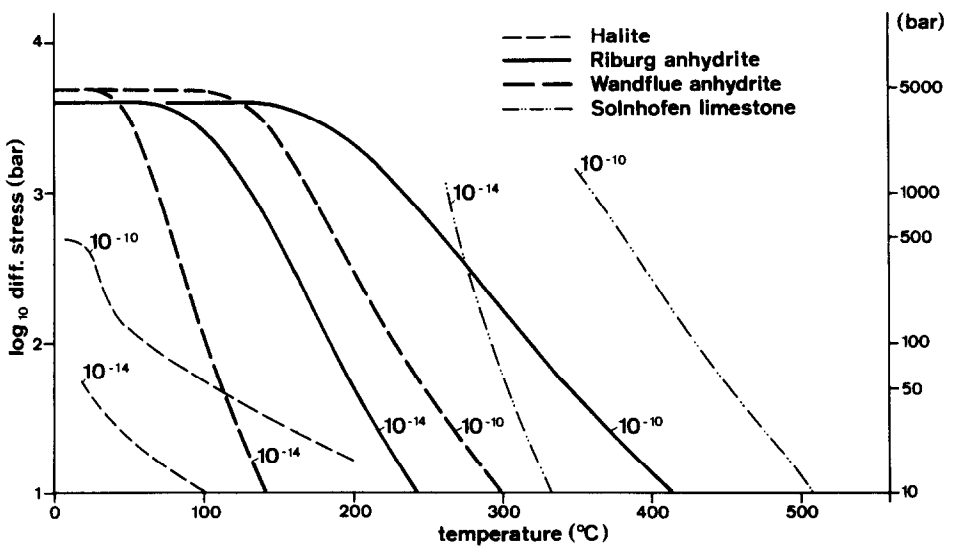

Fig. 13. Synoptic diagram of log stress vs. temperature illustrates the relative strength at 10% strain of halite, anhydrite and limestone expected under geological strain rates. The extrapolations for halite and limestone are based on the flow laws published by Heard (1972) and Schmid et al. (1977).

structural and textural features diagnostic for the deformation mechanism. Since a strong effect of annealing on the microstructure has been detected strong indications may only be gained from textural studies. Both Andreatta (1938) and Schwerdtner (1970) showed that lineated anhydrite rocks have a strong maximum for (010) parallel to the lineation. This is compatible with our findings that the shortening axes are strongly depleted near (010) but this evidence is not sufficient for definite conclusions. Another line of evidence supporting the validity of the laboratory results for geological applications is the observation of Müller and Briegel (1980) that strong deformation is restricted to fine grained layers in cores from the Altishofen drillhole situated in the Swiss molasse basin.

ACKNOWLEDGEMENTS

We are grateful to F. Pirovino for preparing the thin sections and to U. Gerber for photographic reproduction. A. Uhr helped in drawing the figures. We thank M. Casey for providing the texture analysis programs, for all the good discussions and the critical reading of the manuscipt.

REFERENCES

Andreatta, C., 1938. Analisi strutturali di rocco metamorfiche. VII: Anidrite. Period. Mineral., 9: 305—321.

Berner, R.A., 1971. Principals of Chemical Sedimentology. McGraw-Hill, New York, Toronto, London, 240 pp.

Buxtorf, A., 1907. Geologische Beschreibung des Weissenstein-Tunnels und seiner Umgebung. Beitr. Geol. Karte Schweiz (N.F.) 21.

Casey, M., Rutter, E.H., Schmid, S.M., Siddans, A.W.B. and Whalley, G.S., 1978. Texture development in experimentally deformed calcite rocks. In: G. Gottstein and K. Lücke (Editors), Proc. ICOTOM. 5, March 1978, Aachen. 2: 231—240.

Casey, M., 1981. Numerical analysis of X-ray texture data: an implementation in Fortan allowing triclinic or axial specimen symmetry and most crystal symmetries. Tectonophysics, 78: 51—64.

Garofalo, F., 1965. Fundamentals of Creep and Creep-rupture in Metals. McMillan, New York, N.Y., 258 pp.

Guillope, M. and Poirier, J.P., 1979. Dynamic recrystallization during creep of single-crystalline halite. J. Geophys. Res., 84 (B10): 5557—5567.

Handin, J. and Hager, R.V., Jr., 1957. Experimental deformation of sedimentary rocks under confining pressure: Tests at room temperature on dry samples. Bull. Am. Assoc. Pet. Geol., 41: 1—50.

Heard, H.C., 1972. Steady state flow in polycrystalline halite at pressure of 2 kilobars. In: H.C. Heard, I.V. Borg, N.L. Carter and C.B. Raleigh (Editors), Flow and Fracture of Rocks. Geophys. Monogr. Ser., Am. Geophys. Union, 16: 191—210.

Höhne, E., 1963. A more accurate determination of the crystal structure of anhydrite, $CaSO_4$. Sov. Phys. — Crystallogr., 7 (5): 559—569.

Klassen-Neklyudova, M.V., 1964. Mechanical Twinning of Crystals. Consultants Bureau, New York, N.Y., 87 pp.

Laubscher, H.P., 1961. Die Fernschubhypothese der Jurafaltung. Eclogae Geol. Helv., 54: 221—282.

Laubscher, H.P., 1975. Viscous components in Jura folding. Tectonophysics, 27: 239—254.

Müller, P. and Siemes, H., 1974. Festigkeit, Verformbarkeit und Gefügeregelung von Anhydrit. Tectonophysics, 23: 105—127.

Müller, W.H. and Briegel, U., 1977. Experimentelle Untersuchungen an Anhydrit aus der Schweiz. Eclogae Geol. Helv., 70 (3): 685—699.

Müller, W.H. and Briegel, U., 1978. The rheological behaviour of polycrystalline anhydrite. Eclogae Geol. Helv., 71 (2): 397—407.

Müller, W.H. and Briegel, U., 1980. Mechanical aspects of the Jura overthrust. Eclogae Geol. Helv., 73 (1): 239—250.

Müller, W.H. and Hsü, K.J., 1980. Stress distribution in overthrusting slabs and mechanics of Jura deformation. Rock Mech. Suppl., 9: 219—232.

Nicolas, A. and Poirier, J.P., 1976. Crystalline Plasticity and Solid State Flow in Metamorphic Rocks. Interscience, New York, N.Y. 444 pp.

Paterson, M.S., 1978. Experimental Rock Deformation. The Brittle Field, Minerals and Rocks. Springer Verlag, Berlin, Heidelberg, New York, 254 pp.

Ramez, M.R.H., 1976a. Mechanisms of intragranular gliding in experimentally deformed anhydrite. Neues Jahrb. Mineral. Abh., 127 (3): 311—329.

Ramez, M.R.H., 1976b. Fabric changes in experimentally deformed anhydrite rocks. Neues Jahrb. Mineral. Abh., 128 (1): 89—113.

Schmid, S.M., 1976. Rheological evidence for changes in the deformation mechanism of Solnhofen limestone towards low stresses. Tectonophysics, 31: T21—T28.

Schmid, S.M., Boland, J.N. and Paterson, M.S., 1977. Superplastic flow in fine-grained limestone. Tectonophysics, 43: 257—291.

Schmid, S.M., Paterson, M.S. and Boland, J.N., 1980. High temperature flow and dynamic recrystallisation in Carrara Marble. Tectonophysics, 65: 245—280.

Schwerdtner, W.M., 1970. Gitterorientierungs-Mechanismus in Anhydrit-Schiefer. In: P. Paulitsch (Editor), Rock Deformation. Springer Verlag, Berlin, Heidelberg, New York, pp. 142—164.

Spiers, C.J., 1979. Fabric development in calcite polycrystals deformed at 400°C. Bull. Mineral., 102: 282—289.